

SULI Report



July 30, 2012



Search for the Standard Model Higgs boson in the $H \rightarrow Z\gamma$ decay mode at $\sqrt{s} = 7$ and 8 TeV

B. Auerbach^a, S. Chekanov^a, J. Loyal^b

^a*Argonne National Lab, HEP Division, USA*

^b*Duke University, Physics Department, USA*

Abstract

Searches for the Standard Model Higgs boson decaying to the $Z\gamma$ final state in proton-proton collisions at center-of-mass energies of 7 TeV and 8 TeV were performed using 4.9 fb⁻¹ and 5.9 fb⁻¹ of data collected during 2011 and 2012, respectively, recorded with the ATLAS detector located at the Large Hadron Collider in Geneva, Switzerland. Two independent channels were investigated using $Z \rightarrow \mu^+\mu^-$ and $Z \rightarrow e^+e^-$ final states. The main kinematic distributions of the final state products were reconstructed and compared to Standard Model Monte Carlo simulations. Studies of resolution efficiency for the $Z\gamma$ channel were also performed. The sensitivity of the selection criteria was evaluated by plotting the p-value of the background only hypothesis as a function of the $Z\gamma$ mass in a preparation to develop a more sensitive search for the Standard Model Higgs decaying through the $Z\gamma$ channel.

Contents

1	Introduction	2
2	Theoretical predictions	3
3	The ATLAS Detector	5
4	Data and event selection	6
4.1	Description	6
4.2	Selection Results for 2011 and 2012	7
5	Control distributions	7
5.1	Kinematic distributions in 2011 data	7
5.2	Kinematic distributions in 2012 data	12
6	Efficiency and resolution studies	16
7	Results	18
7.1	$Z - \gamma$ mass distributions	18
7.2	Setting the limits	20
8	Conclusions	24

1 Introduction

The Standard Model, the current theoretical framework physicists use to describe the fundamental processes of nature, is responsible for accurately describing three out of the four fundamental forces in nature: the electromagnetic, strong, and weak interactions. The Higgs boson is an essential component of the Standard Model and plays an important role in the predictive power of the theory. Like much of modern physics, the Standard Model relies heavily on the symmetries of nature. Just as concepts such as conservation of momentum and energy can be tied to the fact that a system is symmetric under translations in space and time¹, much of the mathematical framework of the Standard Model is based on internal symmetries known as gauge symmetries. In fact there are three gauge symmetries found in the Standard Model² each of which predicts a force carrying particle that mediates one of the aforementioned interactions of nature. The photon mediates the electromagnetic interaction. The massless gluon is responsible for the strong interaction, which binds quarks together to form protons and neutrons. And finally, the weak interaction, which causes radioactive decays, is mediated by the massive W^\pm and Z bosons. The problem with all of this symmetry is that it predicts that the weak nuclear force is a long range force, something which is not observed in nature. The reason for this discrepancy can be traced back to the fact that the W and Z bosons are not massless particles, but have a mass of roughly 80 and 90 GeV respectively. In addition, these internal gauge symmetries also predict that other fundamental particles, such as the electron, are massless. In order to solve this apparent predicament one needs to introduce a mechanism that keeps the equations that govern the Standard Model's behavior symmetric, but allows for some asymmetric lowest energy states, i.e. 'ground states'. This is accomplished with a theoretical mechanism known as spontaneous symmetry breaking or in this special case the Higgs mechanism.

On July 4th, 2012 the ATLAS and CMS collaborations both announced the discovery of a particle consistent with the Standard Model Higgs boson. With this observed signal at 126 GeV, it is now becoming more and more important to understand the properties of this new scalar particle. The main decay modes being probed in the searches presented on the July 4th announcement are the $H \rightarrow \gamma\gamma$ channel, the $H \rightarrow WW^* \rightarrow 2\ell 2\nu$ channel and the 'golden channel', $H \rightarrow ZZ^* \rightarrow 4\ell$. However, little attention has been paid to the $H \rightarrow Z\gamma \rightarrow \ell^+\ell^-\gamma$ channel despite the fact that its event rate is comparable to that of the golden channel for a 126 GeV Standard Model Higgs boson. The main reason for this is the low branching ratio for $Z \rightarrow \ell^+\ell^-$, the probability that a Z boson will decay into two leptons, which makes the $Z\gamma$ channel statistically limited. Although, the background rate, the number of non-interesting physics processes that contaminate the process of interest, of the $Z\gamma$ channel is higher than that of the $ZZ^* \rightarrow 4\ell$ channel there are a few important properties that make a study of the $Z\gamma$ channel compelling: 1) all final state particles can be measured well with the ATLAS detector; 2) the Higgs mass could be measured from the total invariant mass spectrum; 3) the spin of the Higgs can be studied by analyzing the angular distribution of the decay products, and 4) this channel can be used for setting limits on the Higgs coupling constants. All of these measurements will help to identify this new particle sitting at 126 GeV as a Standard Model Higgs boson or something more exotic.

This report documents the measurements of the production of $Z\gamma$ boson pairs from pp collisions provided by the LHC, focusing on studies of the Higgs to $Z\gamma$ decay channel. This study employs a 'blind approach' in searching for new particles. The approach is blind in the sense that the criteria used to select interesting collision events is not tuned in order to increase the search's sensitivity of detecting the Higgs. Instead the selection cuts used to reconstruct the leptons and photons as well as for selecting interesting events are those used in studies searching exclusively for a $Z\gamma$ final state that is not necessarily required to come from a Higgs boson.

The main purpose of this report is to assess our understanding of the $Z\gamma$ selection process, which

¹ This result is known as Noether's Theorem and can be attributed to the brilliant German mathematician Emmy Noether.

² In group theoretic language the symmetries of the Standard Model can be written as $SU(3) \times SU(2) \times U(1)$.

includes understanding the reconstruction of the leptons and photons from the information provided by the ATLAS detector, the type and shape of the background processes, and the statistical analysis required to find a Higgs. It is for this purpose that we present the kinematic distributions of the three-body final state ($\ell^+\ell^-\gamma$ where ℓ can be an electron or a muon) in comparison with theory predictions. In addition, efficiency and mass resolution studies are conducted and used in a preliminary analysis of the sensitivity of the current selection to a Standard Model Higgs boson.

2 Theoretical predictions

Not only is the Standard Model comparable to the periodic table of particle physics, but it is also a predictive theory. One thing that the Standard Model is able to calculate is the amount of $H \rightarrow Z\gamma$ events, what is called signal in this paper, one expects to see over the course of the experiment. The amount of signal is determined by the following formula:

$$\text{Number}(H \rightarrow \ell^+\ell^-\gamma) = \text{Number}(H \rightarrow X) \times \text{Prob}(H \rightarrow Z\gamma) \times \text{Prob}(Z \rightarrow \mu \text{ or } e) \quad (1)$$

where X can represent any possible Higgs' decay product and the $\text{Prob}(H \rightarrow Z\gamma)$ and $\text{Prob}(Z \rightarrow \mu \text{ or } e)$ are known as branching ratios.

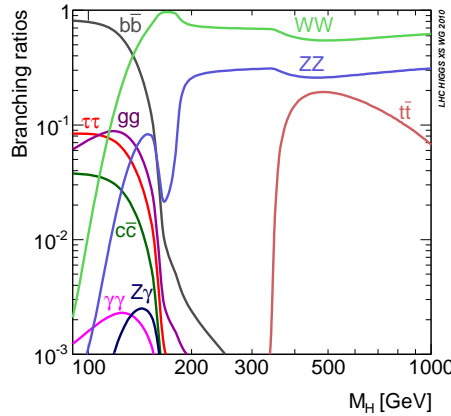


Figure 1: SM Higgs branching ratios as a function of the Higgs-boson mass [1].

The branching ratio of various Higgs decay process as a function of the Higgs' mass is shown in Fig. 1. The branching ratio and therefore the number of expected signal events are roughly comparable for the $H \rightarrow \gamma\gamma$ and the $H \rightarrow Z\gamma$ channels for a 126 GeV Higgs boson, which makes this channel compelling in its likelihood to be sensitive to a signal.

The other quantities in Eq. 1 denoted by $\text{Number}(H \rightarrow X)$ and $\text{Number}(H \rightarrow Z\gamma)$ are proportional to a physical quantity known as a cross-section. Tables 1 and 2 show the Higgs cross sections and branching ratios to the $Z\gamma$ channel as a function of the Higgs mass [1]. At around 125 GeV, the predicted cross section for $H \rightarrow X$ at 7 TeV is $15.74^{+8.6}_{-9.7}$ pb. Taking into account the branching ration at this Higgs mass and the branching ratio of Z to either muons and electrons, the predicted number of Higgs decays is 7

Table 1: Results on $pp \rightarrow H + X$ cross sections at $\sqrt{s} = 7$ TeV

$H(\text{GeV})$	σ	Scale [%]	PDF+ α_S [%]	PDF4LHC [%]
90	30.70	+10.2 -11.9	+4.2 -3.1	+8.0 -6.9
95	27.54	+9.9 -10.8	+4.1 -3.1	+8.0 -6.9
100	24.81	+9.7 -10.5	+4.1 -3.1	+7.9 -7.0
105	22.47	+9.4 -10.3	+4.1 -3.1	+7.9 -7.0
110	20.44	+9.2 -10.1	+4.1 -3.1	+7.9 -7.1
115	18.67	+8.9 -10.0	+4.1 -3.1	+7.9 -7.2
120	17.12	+8.7 -9.8	+4.1 -3.1	+7.8 -7.2
125	15.74	+8.6 -9.7	+4.0 -3.1	+7.8 -7.3
130	14.52	+8.3 -9.6	+4.0 -3.1	+7.8 -7.4
135	13.43	+8.2 -9.4	+4.0 -3.1	+7.7 -7.4
140	12.45	+8.1 -9.3	+4.0 -3.1	+7.8 -7.5
145	11.58	+8.0 -9.3	+4.0 -3.2	+7.8 -7.5
150	10.79	+7.9 -9.3	+4.0 -3.2	+7.8 -7.6
155	10.08	+7.7 -9.2	+4.0 -3.2	+7.7 -7.7
160	9.36	+7.6 -9.2	+4.0 -3.2	+7.7 -7.7
165	8.54	+7.5 -9.2	+4.0 -3.2	+7.7 -7.8
170	7.92	+7.5 -9.2	+4.0 -3.2	+7.7 -7.9

for the 2011 dataset. The production cross-section of a SM Higgs boson with a mass $m_H = 125$ GeV increases by 22% when the center-of-mass energy at the LHC increases from 7 TeV to 8 TeV, leading to 9 ± 2 expected decays.

Table 2: SM Higgs branching ratios to the $Z\gamma$ channel and Higgs total widths in the low- and intermediate-mass range.

M_H [GeV]	$Z + \gamma$	Total Γ_H [GeV]
90	0.00	$2.20 \cdot 10^{-3}$
95	$4.52 \cdot 10^{-6}$	$2.32 \cdot 10^{-3}$
100	$4.98 \cdot 10^{-5}$	$2.46 \cdot 10^{-3}$
105	$1.73 \cdot 10^{-4}$	$2.62 \cdot 10^{-3}$
110	$3.95 \cdot 10^{-4}$	$2.82 \cdot 10^{-3}$
115	$7.16 \cdot 10^{-4}$	$3.09 \cdot 10^{-3}$
120	$1.12 \cdot 10^{-3}$	$3.47 \cdot 10^{-3}$
125	$1.55 \cdot 10^{-3}$	$4.03 \cdot 10^{-3}$
130	$1.96 \cdot 10^{-3}$	$4.87 \cdot 10^{-3}$
135	$2.28 \cdot 10^{-3}$	$6.14 \cdot 10^{-3}$
140	$2.47 \cdot 10^{-3}$	$8.12 \cdot 10^{-3}$
145	$2.49 \cdot 10^{-3}$	$1.14 \cdot 10^{-2}$
150	$2.32 \cdot 10^{-3}$	$1.73 \cdot 10^{-2}$
155	$1.91 \cdot 10^{-3}$	$3.02 \cdot 10^{-2}$
160	$1.15 \cdot 10^{-3}$	$8.29 \cdot 10^{-2}$
165	$5.45 \cdot 10^{-4}$	$2.46 \cdot 10^{-1}$
170	$4.00 \cdot 10^{-4}$	$3.80 \cdot 10^{-1}$

3 The ATLAS Detector

The ATLAS detector [2], see Fig. 2, is one of four detectors located along the 27 km circumference ring of the Large Hadron Collider's (LHC), a particle accelerator located on the border of France and Switzerland. ATLAS is designed to detect a variety of different particles that are produced after the proton beams delivered by the LHC collide at the center of the detector. Roughly 44 meters long and 25 meters in diameter, the ATLAS detector is composed of three distinct layers that help reconstruct the kinematic information contained in the aftermath of the proton-proton collision.

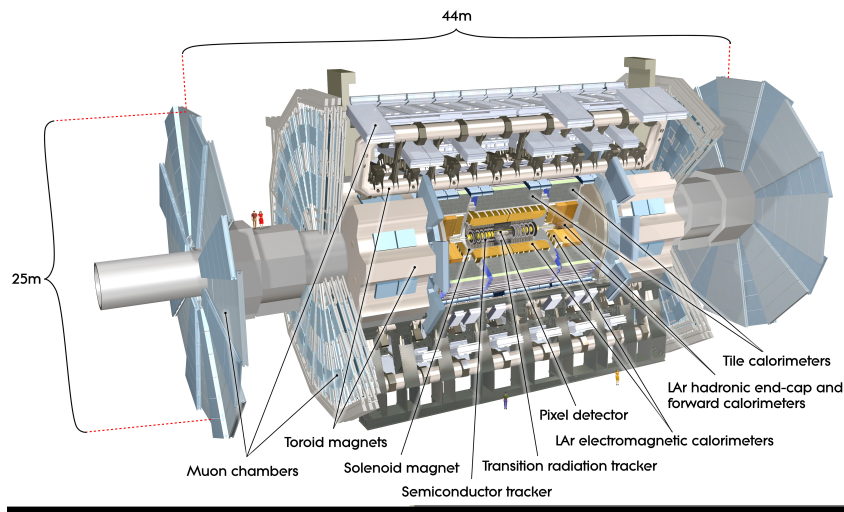


Figure 2: Schematic of the ATLAS detector which is one of the four detectors located at the LHC. Data shown in this report was recorded by the ATLAS detector over two periods of running in 2011 and 2012 respectively.

The analysis presented in this report focuses on the following three kinematic variables associated with a particle: transverse momentum p_T , pseudorapidity η , and azimuthal angle ϕ . These variables

are defined in terms of the coordinate system employed by the ATLAS collaboration. ATLAS uses a right-handed coordinate system with its origin at the point of the proton-proton collision (PC) located at the center of the detector and the z -axis along the beam pipe. The x -axis points from the PC to the center of the LHC ring, and the y -axis points upward. Cylindrical coordinates (r, ϕ) are used in the transverse plane, ϕ being the azimuthal angle around the beam pipe. The pseudorapidity is defined in terms of the polar angle θ as $\eta = -\ln \tan(\theta/2)$. the distance ΔR in the $\eta - \phi$ space is defined as $\Delta R = \sqrt{(\Delta\eta)^2 + (\Delta\phi)^2}$. The transverse momentum p_T is defined as the amount of a particle's momentum that is located in the plane perpendicular to the beam pipe (the x - y plane).

The ATLAS detector has three main layers that serve to measure the aforementioned quantities. The inner most layer is composed of an inner tracking system (ID), which is immersed in a 2 T axial magnetic field and helps identify the charge and momentum of any charged object that passes through. The next layer is composed of the electromagnetic (EM) and hadronic calorimeters. The EM calorimeter measures the total energy of e^+ , e^- , and photons. When charged particles interact with the material they produce showers, also known as Bremsstrahlung, of photons which decay into e^+ , e^- pairs. The number of final e^+ , e^- pairs is proportional to the energy of the initial particle. Similar to the EM calorimeter, the dense material in the hadronic calorimeter produces showers of charged particles whose energy is measured in order to determine the initiating particle's energy. The outer layer consists of the Muon Spectrometer (MS). Only muons and neutrinos make it this far. The MS takes advantage of the muon's charge to reconstruct its tracks; however, the neutrinos remain undetected and show up as missing energy in the detector.

The analysis uses a dataset collected by the ATLAS detector between the middle of April and the end of October 2011 as well as the beginning of April until the middle of June 2012. The 2011 data corresponds to 4.9 fb^{-1} of pp collisions at a center-of-mass energy of $\sqrt{s} = 7 \text{ TeV}$. Likewise, the 2012 runs contain 5.8 fb^{-1} of data collected by the ATLAS experiment at a center-of-mass energy of $\sqrt{s} = 8 \text{ TeV}$.

4 Data and event selection

4.1 Description

Only events where both the calorimeter and the inner detector are fully operational, and have good data quality are used. The Z candidates are selected exclusively through their decays into e^+e^- and $\mu^+\mu^-$ pairs, and the $Z\gamma$ final state is required to contain one e^+e^- or $\mu^+\mu^-$ pair and an isolated photon.

An electron candidate is obtained by examining the energy deposited in the EM calorimeter, which can be associated with a reconstructed charged particle in the ID. We require the electron's transverse energy to be greater than 25 GeV. In addition, a requirement that the electron satisfies $1.52 < |\eta| < 2.37$ is enforced. Two oppositely charged electrons are required when selecting the $e^+e^-\gamma$ final state. The dominant source of background for the selection of a $Z\gamma$ final state is $Z + \text{jets}$. In order to reduce this background process, which can be caused by misidentifying a jet as an electron, a calorimeter based isolation requirement of $e_T^{iso} < \epsilon \text{ GeV}$ is applied to each electron candidate. We define e_T^{iso} as the fraction of the total transverse energy recorded in the calorimeters within a cone of radius ΔR around the electron direction, while excluding the energy from the electron cluster itself. For 2011 ΔR is required to be less than 0.3, while the cutoff variable ϵ is defined to be 0.14. In 2012 the isolation requirement is loosened to a cone of $\Delta R = 0.2$ and ϵ is set equal to 0.3. It should be noted that E_T^{iso} is corrected for leakage of the electron energy outside the electron cluster and from any additional energy contributions from the underlying event pile-up.

The identification of muon candidates is performed by associating tracks in the MS to tracks in the ID. The muons of interest are combined tracks with transverse momentum $p_T > 25 \text{ GeV}$ and $|\eta| < 2.4$.

The $(Z \rightarrow \mu^+\mu^-)\gamma$ events are required to have exactly two oppositely charged muon candidates. In order to remove any misidentified muons, the following isolation requirement is imposed on the muons: $K_T^{iso} < 0.1$. Here K_T^{iso} is defined to be the sum of the track p_T in a cone of $\Delta R = 0.2$ around the muon direction divided by the muon's p_T .

The discriminating variables used to identify photon candidates utilize clustered energy deposits in the EM calorimeter with $E_T > 15$ GeV. The photon candidates are also required to fall in the range $|\eta| < 2.37$, while excluding the calorimeter transition region $1.37 < |\eta| < 1.52$. A major concern in these analysis is the elimination of background produced by meson decays (e.g $\pi^0 \rightarrow \gamma\gamma$), which are responsible for an abundance of photon fakes. In order to reduce this background, a photon isolation requirement of $E_T^{iso} < 6$ GeV is applied. Similar to the electron isolation, the isolation variable E_T^{iso} is the total transverse energy recorded in the calorimeters within a cone of radius $\Delta R < 0.3$ around the photon direction, while excluding the energy from the photon cluster itself.

Since this analysis is designed as a preliminary analysis for a $H \rightarrow Z\gamma$ search, any final state radiation (FSR) of a photon off of a Z 's daughter lepton is of no interest. In order to suppress any contributions of FSR photons to the Z decays, we required a $\Delta R(\ell, \gamma) > 0.7$ on the final state particles.

4.2 Selection Results for 2011 and 2012

Tables 3 and 4 document the number of events that made it through the overall event selection. Out of the entire data set only 0.7% events remain in 2011 and 0.07% are left in 2012.

Description	Number of Events Remaining
Before any cuts	368907
After all cuts	2551

Table 3: A summary of the overall event selection for the analysis performed on the 2011 data set. The left column presents the point in the analysis and the right column contains the number of events that are still present in the event. Overall, two good quality leptons with opposite charges and $p_T > 25$ GeV were required to be present in the event. In addition, the event had to have an isolated photon with $p_T > 15$ GeV. Out of the entire sample presented only 0.7% remains after all selection criteria are imposed.

Description	Number of Events Remaining
Before any cuts	4585452
After all cuts	3393

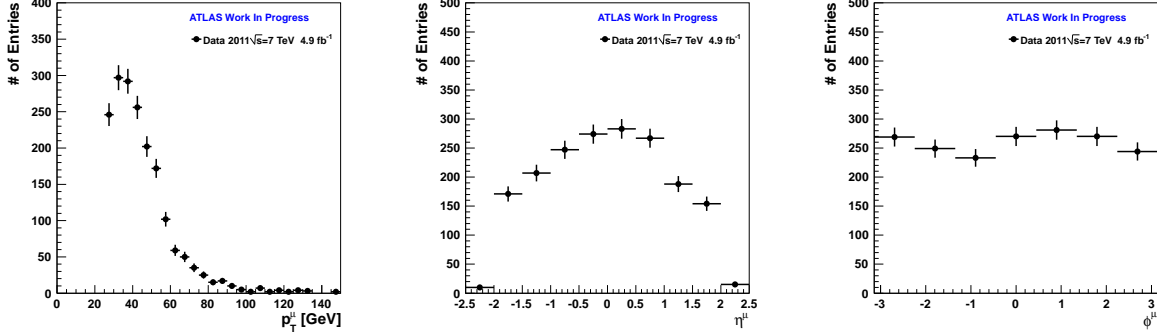
Table 4: A summary of the overall event selection for the analysis performed on the 2012 data set. The left column presents the point in the analysis and the right column contains the number of events that are still present in the event. Overall, two good quality leptons with opposite charges and $p_T > 25$ GeV were required to be present in the event. In addition, the event had to have an isolated photon with $p_T > 15$ GeV. Out of the entire sample presented only 0.07% remains after all selection criteria are imposed.

5 Control distributions

5.1 Kinematic distributions in 2011 data

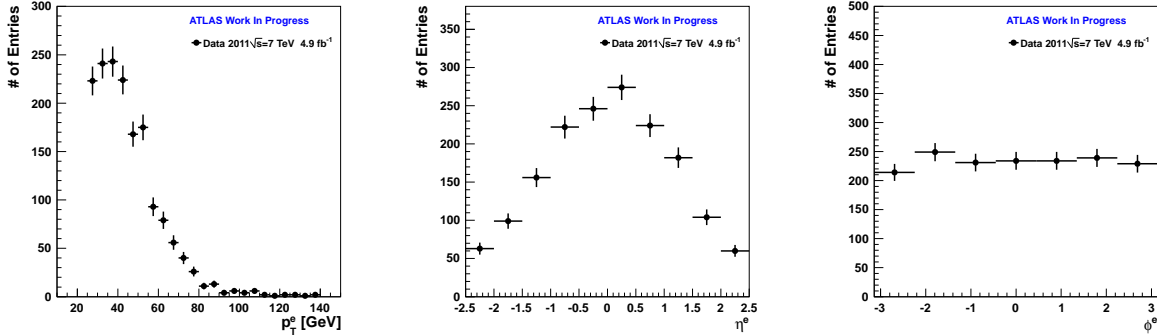
After the appropriate final states were selected from the data a few kinematic distributions were examined in order to determine if our selection process was adequate. These control distributions were analyzed with respect to their known shapes in order to serve as a sanity check for the reconstruction of the final state particles.

With this in mind, Figures 3 and 4 shows several control distributions for electrons and muons used in the analysis of the 2011 data set. As a rule of thumb one expects the p_T spectrum of the leptons to decay exponentially with increasing transverse momentum, the η spectrum to peak at the transverse plan, i.e. $\eta = 0$, and the distributions in ϕ to be roughly uniform.



(a) p_T^μ distribution for data taken in 2011. (b) η^μ distribution for data taken in 2011. (c) ϕ^μ distribution for data taken in 2011.

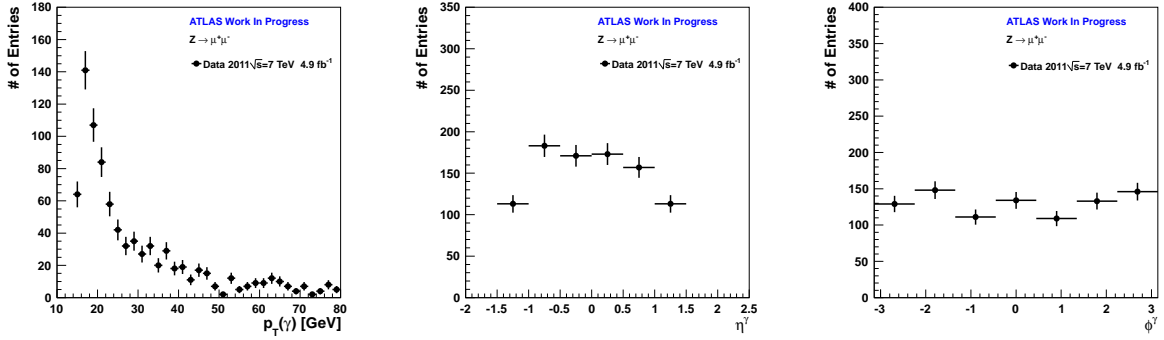
Figure 3: Kinematic Distribution of the muons from $Z\gamma$ decays in the 2011 data. The muons are required to pass all selection criteria. (a) presents the p_T spectrum of the muon where the muon is required to have transverse momentum greater than 25 GeV. In (b) the muon is required to have an η value less than 2.4.



(a) p_T^e spectrum for data taken in 2011. (b) η^e distribution for data taken in 2011. (c) ϕ^e distribution for data taken in 2011.

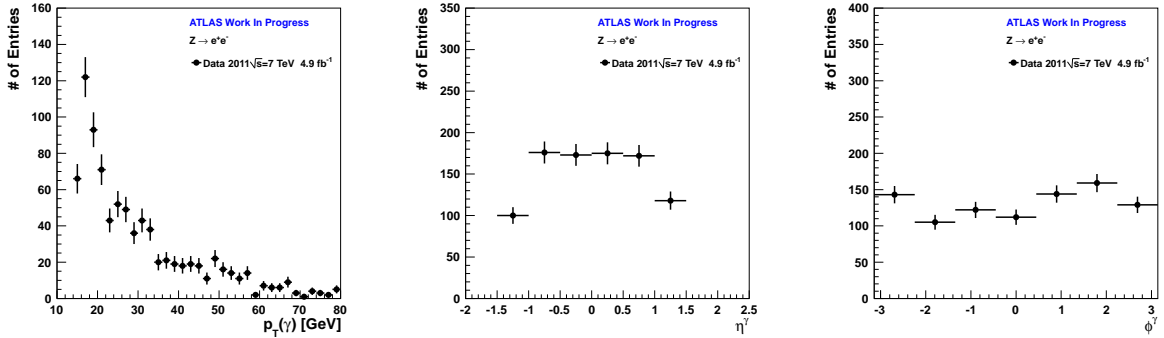
Figure 4: Kinematic Distribution of the electrons from $Z\gamma$ decays in the 2011 data. The electrons are required to pass all selection criteria. (a) presents the p_T spectrum of the electron where the electron is required to have transverse momentum greater than 25 GeV. In (b) the electron is required to have an η value between 1.52 and 2.47.

The distributions for the photons are in Fig. 5 and 6, which present the muons and electron channels, respectively. Since the final state of interest can be either $e^+e^- \gamma$ or $\mu^+\mu^-\gamma$, the photon distributions were split up according to the leptons present in the event, which allows us to tag a given photon with the associated decay process.



(a) $p_T(\gamma)$ distribution (Muon Channel) (b) $\eta(\gamma)$ distribution (Muon Channel) (c) $\phi(\gamma)$ distribution (Muon Channel)

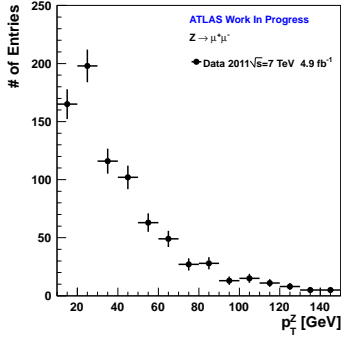
Figure 5: Kinematic Distribution of the photons present in events with a $Z \rightarrow \mu^+\mu^-$ in the 2011 data. The photons are required to pass all selection criteria. (a) presents the p_T spectrum of the photon where the photon is required to have transverse momentum greater than 15 GeV. In (b) the photon is required to have an η value between 1.52 and 2.37 (excluding the crack region).



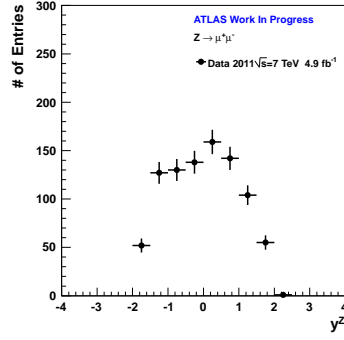
(a) $p_T(\gamma)$ distribution (Electron Channel) (b) $\eta(\gamma)$ distribution (Electron Channel) (c) $\phi(\gamma)$ distribution (Electron Channel)

Figure 6: Kinematic Distribution of the photons present in events with a $Z \rightarrow e^+e^-$ in the 2011 data. The photons are required to pass all selection criteria. (a) presents the p_T spectrum of the photon where the photon is required to have transverse momentum greater than 15 GeV. In (b) the photon is required to have an η value between 1.52 and 2.37 (excluding the crack region).

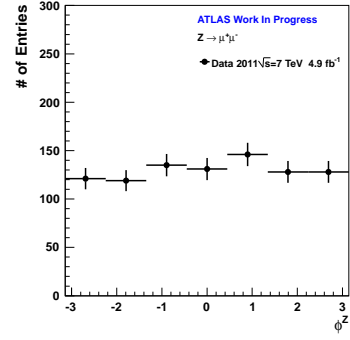
Finally the the kinematic distributions of the Z bosons associated with the two leptons are given in Fig. 7 and Fig. 18. The p_T , η , ϕ distributions for the Z should have the same shape as the distributions of the leptons. In addition, the mass spectrum of the Z boson is plotted using the kinematic information of the leptons. The peak at 70 GeV is the result of a Z decaying into two leptons and a photon, i.e. $Z \rightarrow \ell^+ \ell^- \gamma$ and is not a process of interest. The peak at roughly 90 GeV, the mass of the Z , corresponds to a purely leptonic decay, i.e. $Z \rightarrow \ell^+ \ell^-$, and may be part of a $H \rightarrow Z\gamma$ event. The white histogram that is overlaid on the mass plot corresponds to the distribution predicted by theory. As before the distributions are split according to the leptons present in the event.



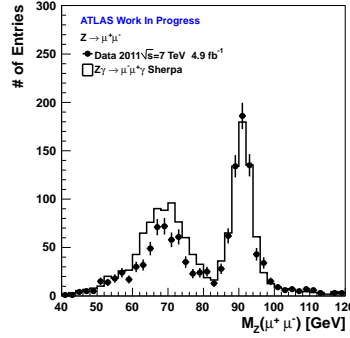
(a) $p_T(Z)$ distribution (Muon Channel)



(b) $y(Z)$ distribution (Muon Channel)

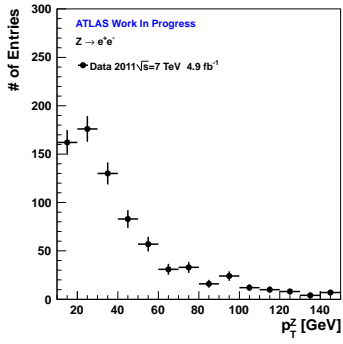


(c) $\phi(Z)$ distribution (Muon Channel)

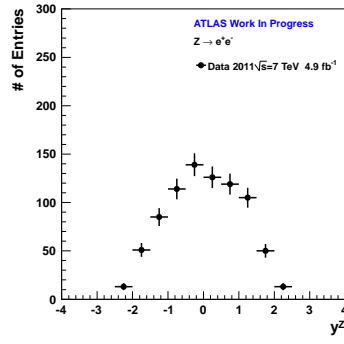


(d) m_Z distribution (Muon Channel)

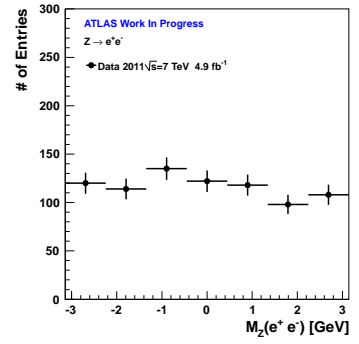
Figure 7: Kinematic Distribution of the Z bosons decaying into two muons for the 2011 data. The Z 's are taken from events passing all selection criteria



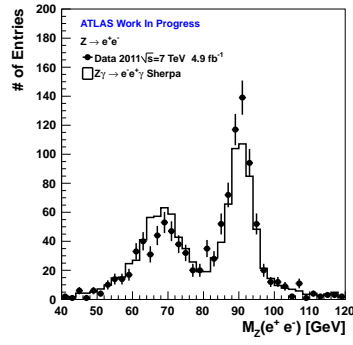
(a) $p_T(Z)$ distribution (Electron Channel)



(b) $y(Z)$ distribution (Electron Channel)



(c) $\phi(Z)$ distribution (Electron Channel)

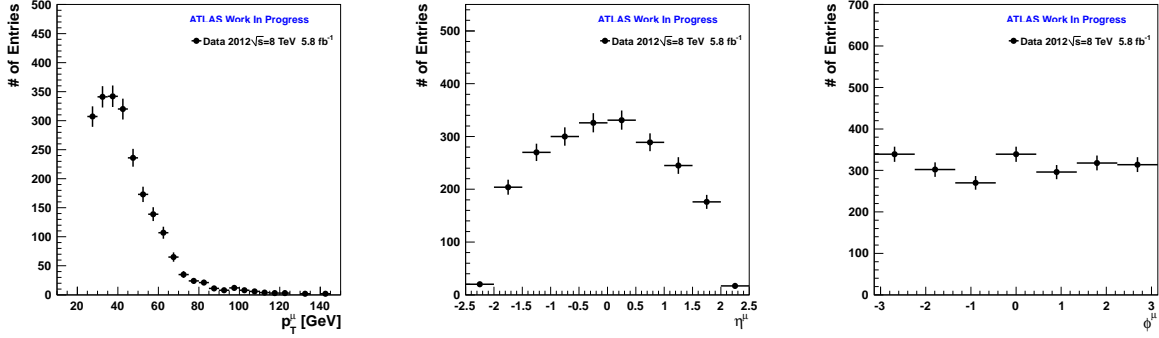


(d) m_Z distribution (Electron Channel)

Figure 8: Kinematic Distribution of the Z bosons decaying into two electrons for the 2011 data. The Z 's are taken from events passing all selection criteria

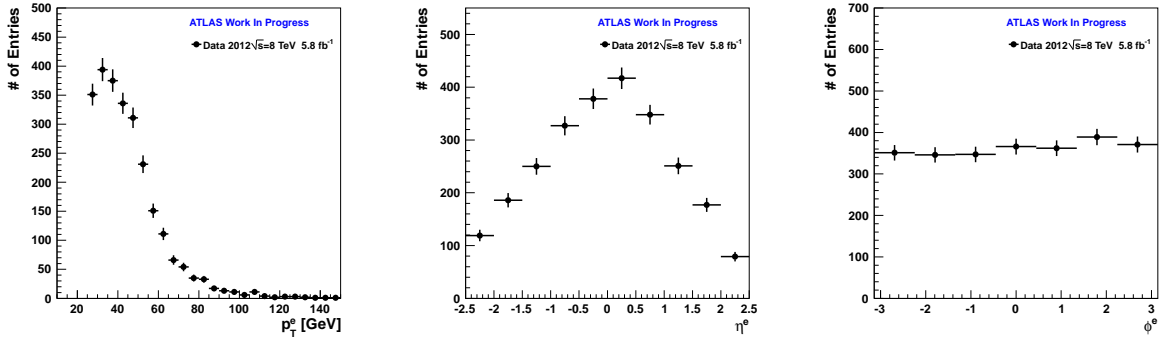
5.2 Kinematic distributions in 2012 data

Figures 9 and 10 shows several control distributions for electrons and muons utilized in this analysis using the 2012 data set. The distributions for photons are given in Fig. 11 and 12 for the muons and electron channels, respectively. Finally, the Z distributions are given in Fig. 13 and Fig. 19.



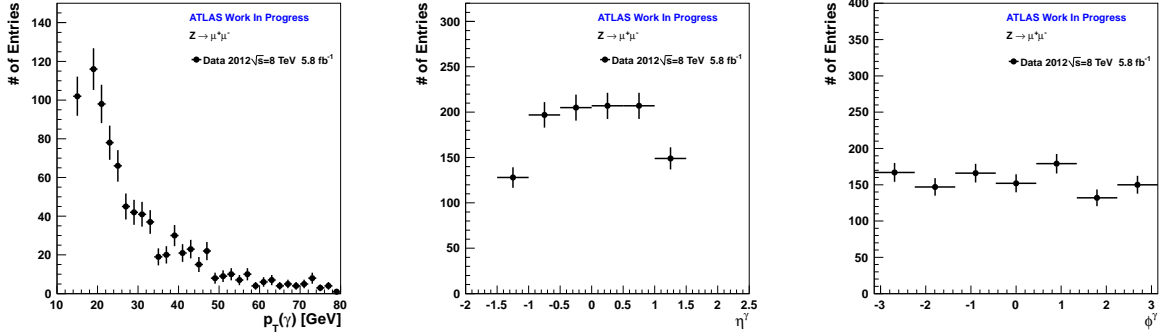
(a) p_T^μ distribution for data taken in 2012. (b) η^μ distribution for data taken in 2012. (c) ϕ^μ distribution for data taken in 2012.

Figure 9: Kinematic Distribution of the muons from $Z\gamma$ decays in the 2012 data. The muons are required to pass all selection criteria. (a) presents the p_T spectrum of the muon where the muon is required to have transverse momentum greater than 25 GeV. In (b) the muon is required to have an η value less than 2.4.



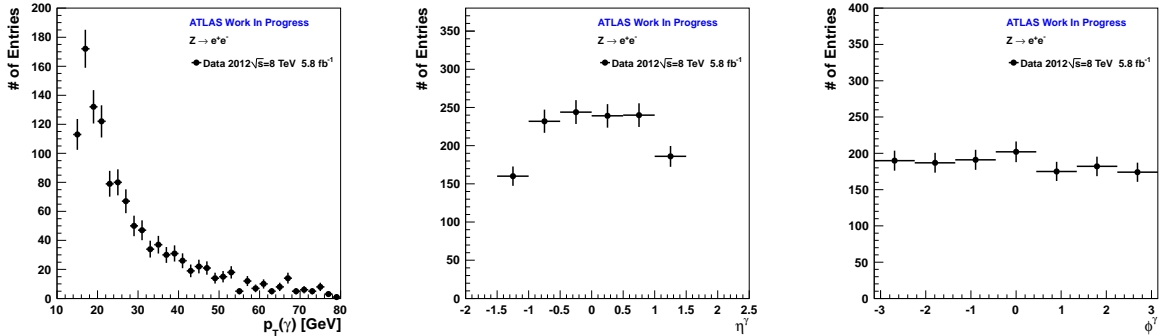
(a) p_T^e spectrum for data taken in 2012. (b) η^e distribution for data taken in 2012. (c) ϕ^e distribution for data taken in 2012.

Figure 10: Kinematic Distribution of the electrons from $Z\gamma$ decays in the 2012 data. The electrons are required to pass all selection criteria. (a) presents the p_T spectrum of the electron where the electron is required to have transverse momentum greater than 25 GeV. In (b) the electron is required to have an η value between 1.52 and 2.47.



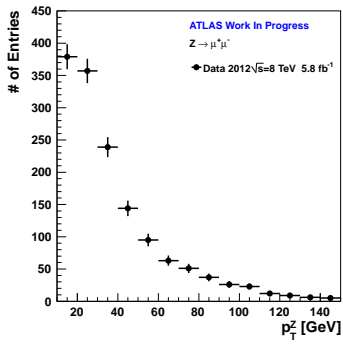
(a) $p_T(\gamma)$ distribution (Muon Channel) (b) $\eta(\gamma)$ distribution (Muon Channel) (c) $\phi(\gamma)$ distribution (Muon Channel)

Figure 11: Kinematic Distribution of the photons present in events with a $Z \rightarrow \mu^+\mu^-$ in the 2011 data. The photons are required to pass all selection criteria. (a) presents the p_T spectrum of the photon where the photon is required to have transverse momentum greater than 15 GeV. In (b) the photon is required to have an η value between 1.52 and 2.37 (excluding the crack region).

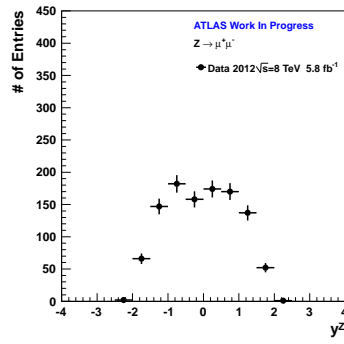


(a) $p_T(\gamma)$ distribution (Electron Channel) (b) $\eta(\gamma)$ distribution (Electron Channel) (c) $\phi(\gamma)$ distribution (Electron Channel)

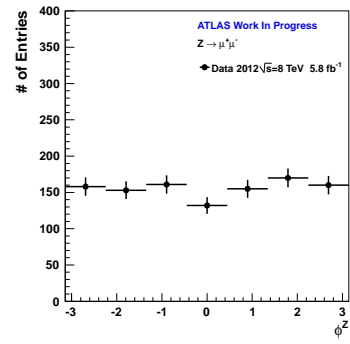
Figure 12: Kinematic Distribution of the photons present in events with a $Z \rightarrow e^+e^-$ in the 2012 data. The photons are required to pass all selection criteria. (a) presents the p_T spectrum of the photon where the photon is required to have transverse momentum greater than 15 GeV. In (b) the photon is required to have an η value between 1.52 and 2.37 (excluding the crack region).



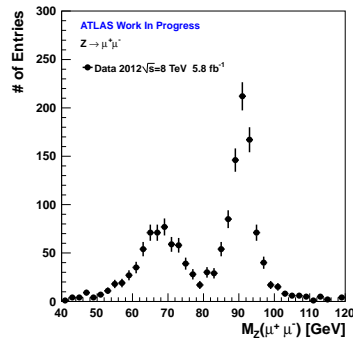
(a) $p_T(Z)$ distribution (Muon Channel)



(b) $y(Z)$ distribution (Muon Channel)

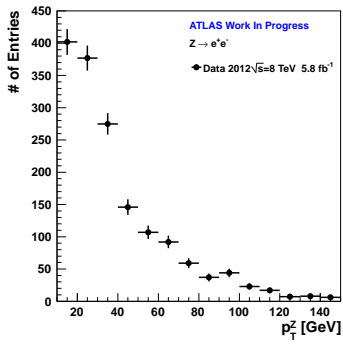


(c) $\phi(Z)$ distribution (Muon Channel)

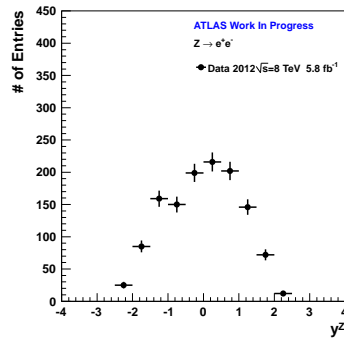


(d) m_Z distribution (Muon Channel)

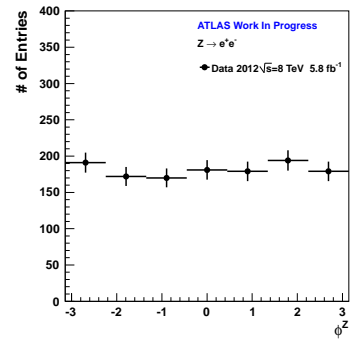
Figure 13: Kinematic Distribution of the Z bosons decaying into two muons for the 2012 data. The Z 's are taken from events passing all selection criteria



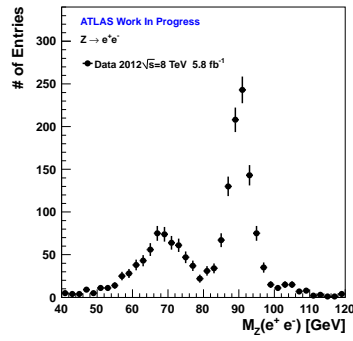
(a) $p_T(Z)$ distribution (Electron Channel)



(b) $y(Z)$ distribution (Electron Channel)



(c) $\phi(Z)$ distribution (Electron Channel)

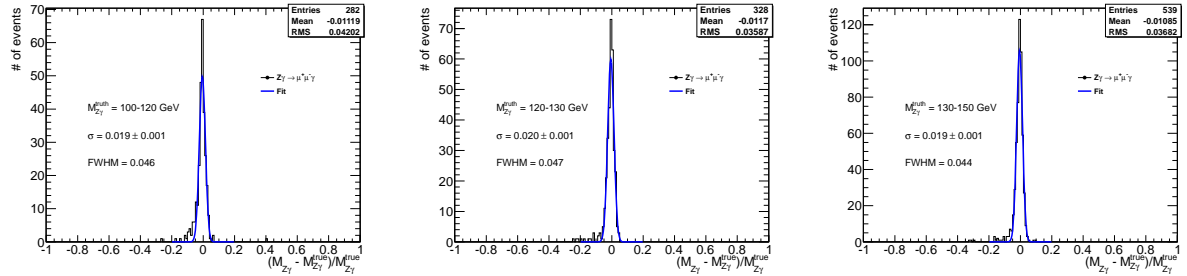


(d) m_Z distribution (Electron Channel)

Figure 14: Kinematic Distribution of the Z bosons decaying into two electrons for the 2012 data. The Z 's are taken from events passing all selection criteria

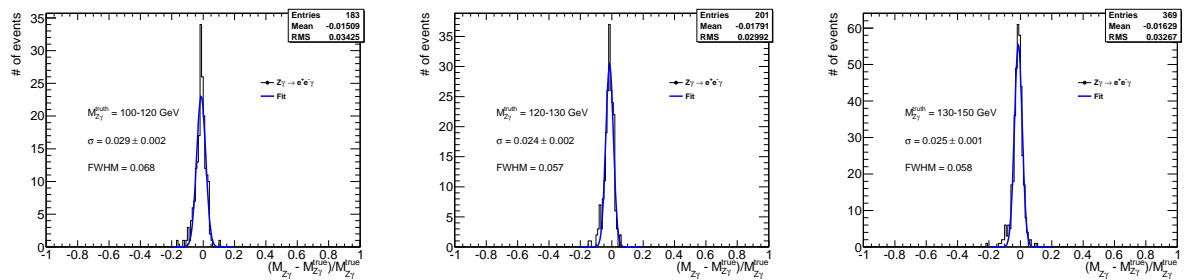
6 Efficiency and resolution studies

There is always some error in the measurement of a particle's kinematic information. As a result the mass that is measured by the experiment can differ from the particle's true mass. Simulated experiments were used to quantify the variance in the $Z\gamma$'s measured mass. Overall the study, which is displayed in Figures 15 and 16, indicates that the final state mass can shift by up to 6% of its true value.



(a) Mass resolution when the true $Z\gamma$ mass lies between 100 and 120 GeV. For this range the mass resolution is 4.6%. (b) Mass resolution when the true $Z\gamma$ mass lies between 120 and 130 GeV. For this range the mass resolution is 4.7%. (c) Mass resolution when the true $Z\gamma$ mass lies between 130 and 150 GeV. For this range the mass resolution is 4.4%.

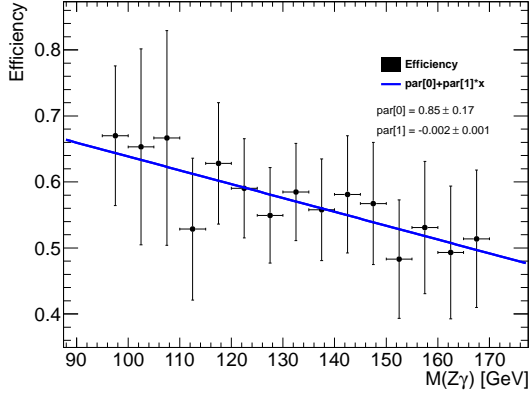
Figure 15: The mass resolution for various values of the true $Z\gamma$ mass in the muon decay mode. A Gaussian is fit to the distribution and the full width at half maximum (FWHM) is extracted from the fit.



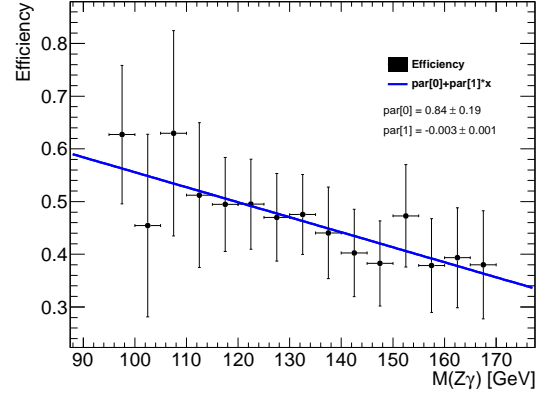
(a) Mass resolution when the true $Z\gamma$ mass lies between 100 and 120 GeV. For this range the mass resolution is 6.8%. (b) Mass resolution when the true $Z\gamma$ mass lies between 120 and 130 GeV. For this range the mass resolution is 5.7%. (c) Mass resolution when the true $Z\gamma$ mass lies between 130 and 150 GeV. For this range the mass resolution is 5.8%.

Figure 16: The mass resolution for various values of the true $Z\gamma$ mass in the electron decay mode. A Gaussian is fit to the distribution and the full width at half maximum (FWHM) is extracted from the fit.

The methods used to select the leptons and photons that can be traced back to the original Higgs decay are not perfect and are not expected to be 100% efficient in selecting every $H \rightarrow Z\gamma$ decay that occurs in the data. In order to determine the selection's efficiency simulated experiments were used to determine the percentage of true signal events that failed to be picked up by the proposed selection. Fig. 17 displays the efficiency for various values of the $Z\gamma$ mass. Tables 5 and 6 display the results of the linear fit applied to the aforementioned results. The efficiency is roughly 50% for each channel.



(a) Efficiency for the muon channel.



(b) Efficiency for the electron channel.

Figure 17: Efficiency studies performed using mc11 Monte-Carlo. The blue line represents the best fit value to the data. Note that the data is assumed to obey gaussian statistics in each bin.

$M_{Z\gamma}$ [GeV]	Efficiency
95	0.65
100	0.64
105	0.63
110	0.62
115	0.61
120	0.60
125	0.59
130	0.58
135	0.57
140	0.55
145	0.54
150	0.53
155	0.52
160	0.51
165	0.50

Table 5: Efficiency values taken from the best linear regression (muon Channel)

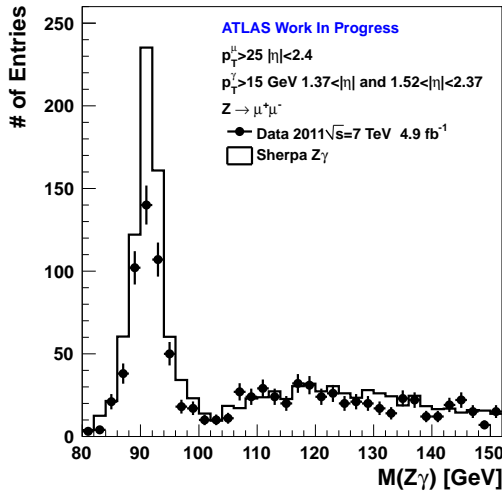
$M_{Z\gamma}$ [GeV]	Efficiency
95	0.57
100	0.56
105	0.54
110	0.53
115	0.51
120	0.50
125	0.48
130	0.47
135	0.46
140	0.44
145	0.43
150	0.41
155	0.40
160	0.38
165	0.37

Table 6: Efficiency values taken from the best linear regression (electron Channel)

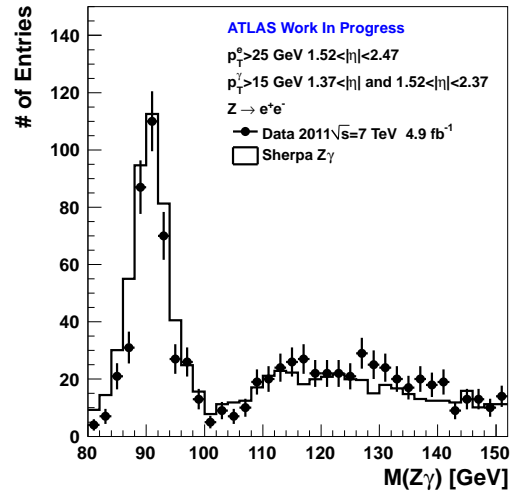
7 Results

7.1 $Z - \gamma$ mass distributions

The main focus of the current studies is the $Z\gamma$ mass distributions which represent the main observables for searches of a Higgs in the $Z\gamma$ decay channel. Figures 18 and 19 show the mass distributions for the muon and electron channels in 2011 and 2012. No significant excess near the 126 GeV region has been found.

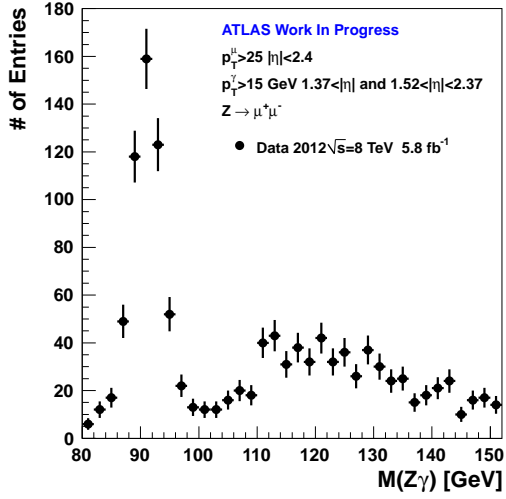


(a) $m(Z\gamma)$ distribution (Muon Channel)

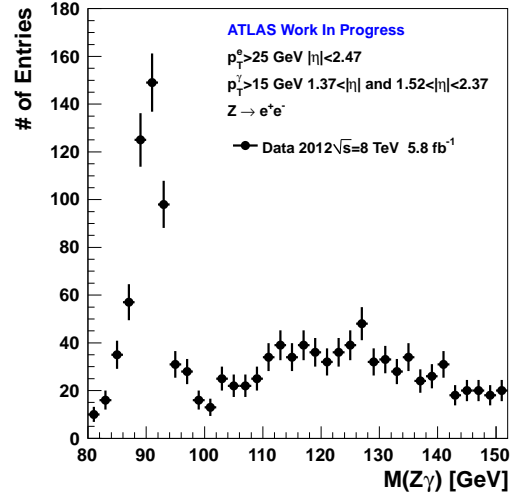


(b) $m(Z\gamma)$ distribution (Electron Channel)

Figure 18: Invariant mass distribution of the three body system ($\ell^+ \ell^- \gamma$) for $\ell = \mu$ (a) and $\ell = e$ (b) in the 2011 data



(a) $m(Z\gamma)$ distribution (Muon Channel)

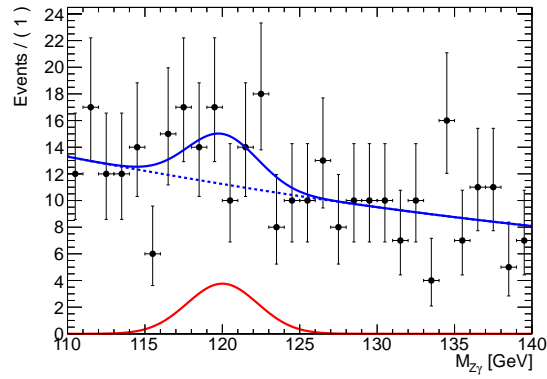


(b) $m(Z\gamma)$ distribution (Electron Channel)

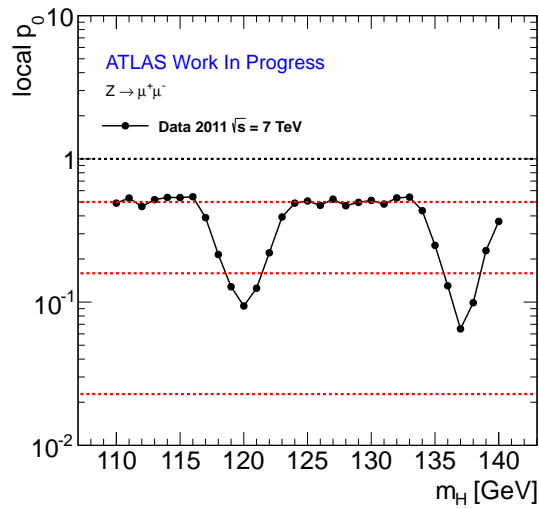
Figure 19: Invariant mass distribution of the three body system ($\ell^+\ell^-\gamma$) for $\ell = \mu$ (a) and $\ell = e$ (b) in the 2011 data

7.2 Setting the limits

In order to determine the sensitivity of the selection criteria to the Higgs decaying into a $Z\gamma$ final state, the p-value of the background only hypothesis as a function of the $Z\gamma$ mass was calculated. A one-sided profile likelihood was used as the test statistic. The results are given in Figures 20 - 23 for both 2011 and 2012 data. The results are split between electron and muon decay channels.

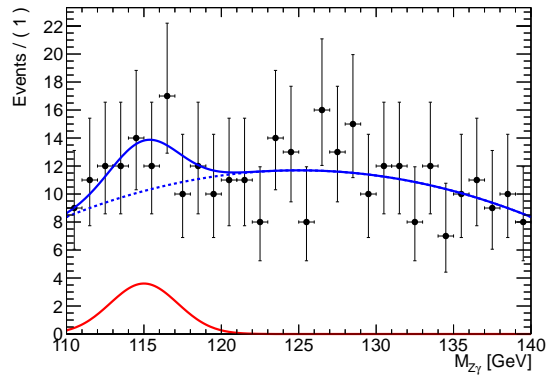


(a) Example fit at 120 GeV

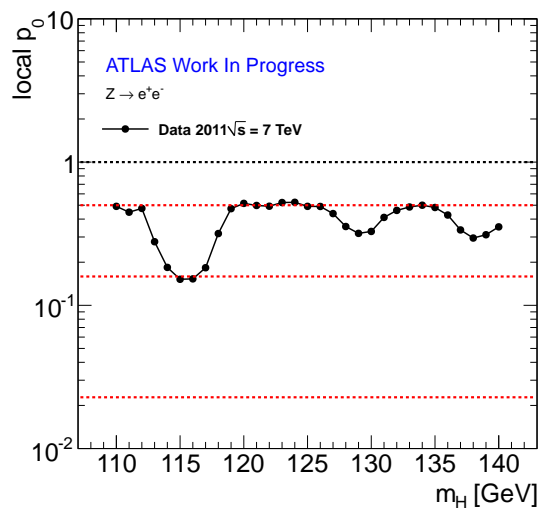


(b) p-value as a function of m_H

Figure 20: p-value for the background only hypothesis in the 2011 data (Muon Channel).

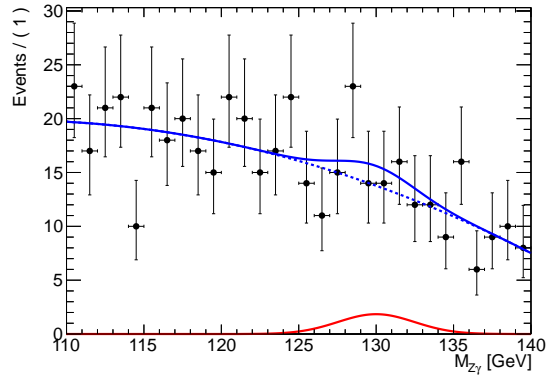


(a) Example Fit at 115 GeV

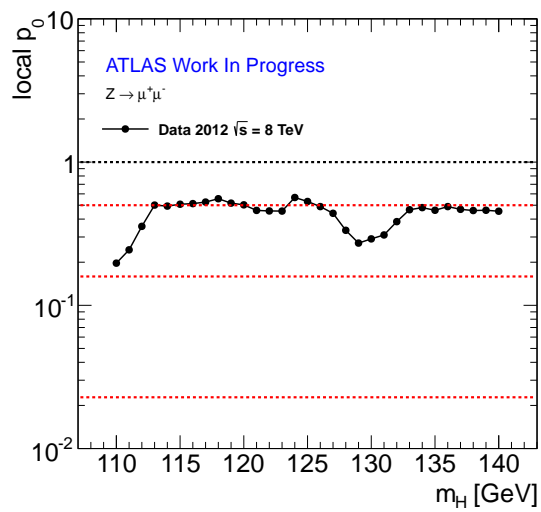


(b) p-value as a function of m_H

Figure 21: p-value for the background only hypothesis in the 2011 data (Electron Channel).

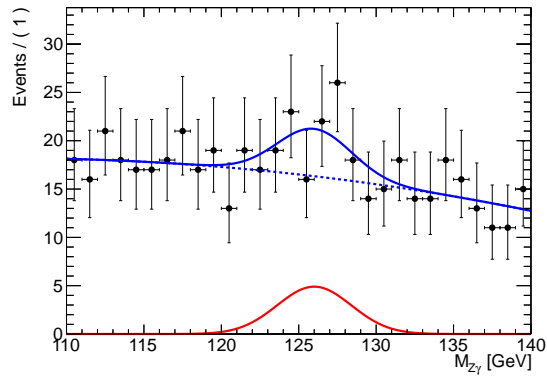


(a) Example fit at 130 GeV

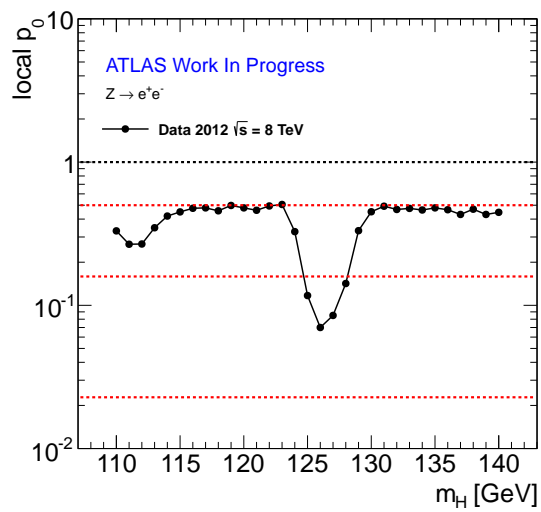


(b) p-value as a function of m_H

Figure 22: p-value for the background only hypothesis in the 2012 data (Muon Channel).



(a) Example Fit at 126 GeV



(b) p-value as a function of m_H

Figure 23: p-value for the background only hypothesis in the 2012 data (Electron Channel).

8 Conclusions

This study is based on 4.9 fb^{-1} and 5.9 fb^{-1} of ATLAS data corresponding to pp collisions at a center-of-mass energy of $\sqrt{s} = 7 \text{ TeV}$ and 8 TeV respectively. The selection of $Z\gamma$ boson pairs was studied in preparation for a search for the Higgs boson decaying into the $Z\gamma$ channel. The measurements have been made using the $\ell^+\ell^-\gamma$ final state where the charged leptons correspond to either an electron or a muon and the photons are required to be isolated. In order to validate the methods used to select $Z\gamma$ events, the various distributions of the kinetic variables of the leptons and photons were analyzed as control distributions. In addition, the mass spectrum of the Z boson was compared to the distributions predicted by theory simulations for 2011 data only. It was found that the distributions are in relatively good agreement with theory.

In order to determine the quality of the selection process the mass resolution and efficiency were calculated using theory simulations. It was found that the muon channel has a mass resolution of 4.7%, while the electron channel has a spread in the reconstructed mass of 6%. The efficiency measurements found that the muon channel had a downward sloping efficiency as a function of mass that was roughly 60%. The electron channel's efficiency also had a downward slope and a value of 50%.

A search for a Higgs boson requires looking for a bump in the mass distribution of the $Z\gamma$ system. This mass distribution was plotted for both the 2011 and 2012 data sets. No significant excess near the 126 GeV region has been found in any of the distributions. The 2011 data was compared with theory simulations and found to be in good agreement. The muon channel is slightly lower than the predicted value at the Z boson peak and will be studied further.

Finally, a p-value scan as a function of the Higgs' mass was performed in order to look for a statistically significant excess in the data. Only 1σ fluctuations were found, which does not allow us to make any concrete statements regarding the presence of the Higgs in the data. However, the results presented here are compatible with a 126 GeV Higgs.

Acknowledgements

We thank the DOE SULI Program for providing the resources necessary to conduct this research, as well as Argonne National Laboratory without whom this research would not be possible. In addition, we thank all the support staff from our home institutions which have been instrumental in assuring the success of this research project.

References

- [1] LHC Higgs Cross Section Working Group Collaboration, S. Dittmaier et al., *Handbook of LHC Higgs Cross Sections: 1. Inclusive Observables*, [arXiv:1101.0593](https://arxiv.org/abs/1101.0593) [hep-ph].
- [2] ATLAS Collaboration, G. Aad et al., *The ATLAS Experiment at the CERN Large Hadron Collider*, JINST **3** (2008) S08003.